PERGAMON

International Journal of Solids and Structures 38 (2001) 8235–8258

INTERNATIONAL JOURNAL OF SOLIDS and STRUCTURES

www.elsevier.com/locate/ijsolstr

Near-tip fields for quasi-static crack growth along the interface between a porous-ductile material and a rigid substrate

Enrico Radi [a,*], M. Cristina Porcu [b]

[a] *Dipartimento di Scienze e Metodi dell'Ingegneria, Università di Modena e Reggio Emilia, Viale Allegri 13, 42100 Reggio Emilia, Italy*
[b] *Dipartimento di Ingegneria Strutturale, Università di Cagliari, Piazza D'Armi, 09123 Cagliari, Italy*

Received 20 November 2000; in revised form 25 May 2001

Abstract

A numerical asymptotic solution is provided for stress and velocity fields near the tip of an interface crack steadily propagating between a porous elastic–plastic material and a rigid substrate, under plane strain conditions. The constitutive description of the ductile material is defined by the Gurson model with constant and uniform porosity, both for isotropic hardening and for perfectly plastic behavior as a limit case. Solutions are obtained by numerically integrating the field equations within elastic and plastic asymptotic sectors and by imposing full stress and velocity continuity. If the hardening coefficient is lower than a critical value two distinct kinds of solution can be found in variable-separable form, corresponding to predominantly tensile or shear mixed mode.

The elastic–perfectly plastic solution is constructed by means of an appropriate assembly of generalized centered fan and non-singular plastic sectors and an elastic unloading sector. The results show that the porosity mainly influences the stress fields of the tensile mode rather than the shear mode, due to the higher hydrostatic stress level. In particular, for high porosities the maximum of the hoop stress deviates from the interface line ahead of the crack-tip, causing possible kinking of the crack trajectory. The performed analysis of the debonding process of this kind of interface is essential for the determination of the overall strength, toughness and reliability of many advanced composite materials and structural components. © 2001 Elsevier Science Ltd. All rights reserved.

Keywords: Fracture mechanics; Interface crack propagation; Elastic–plastic material; Porous material; Asymptotic analysis

1. Introduction

Interfaces between porous ductile and stiffer materials are common in many advanced engineering components, which are obtained by compaction and sintering of metal and ceramic powders or formed by multi-layer substrates (Bordia and Raj, 1985), like modern structural metallic/ceramic composites and packaging structures for electronic devices. Such interfaces also appear in metallic foam core sandwich

* Corresponding author. Tel.: +39-522-276613; fax: +39-522-276603.
E-mail addresses: eradi@unimo.it (E. Radi), mcporcu@hotmail.com (M.C. Porcu).

0020-7683/01/$ - see front matter © 2001 Elsevier Science Ltd. All rights reserved.
PII: S0020-7683(01)00142-1

structures (McCormack et al., 2001) as well as in high-performance metal components obtained by combining the processes of selective laser sintering and hot isostatic pressing (Das et al., 1998). These components consist of a full dense integral skin wrapping a porous core formed from the same material, but with a different microstructure. Again, interfaces of this kind may occur in protective coatings of sintered metal parts, where thin, hard, wear-resistant layers of titanium nitride (TiN), titanium carbonitride (TiC), alumina (Al_2O_3) or zirconia (ZnO), are deposited on the surface of sintered components in order to protect them from wear, high temperatures, chemical attack and corrosion. The use of protective coatings has been largely increased over the last few years, because it may enhance the performance and extend the service life of many advanced structural components. In particular, protective coatings have been intensively used in a wide area of industrial applications, which ranges from gas turbine technology to aircraft and electronics industries, including several engineering applications, like filters, bearings, pumps, compressors, gears and cutting and forming tools. As well known, the mechanical properties of layered composites on a macroscopic scale largely depend on the adhesion and microstructure of the interfaces, since a commonly encountered kind of damage in their failure is represented by slow, stable crack propagation along the interface, which may eventually deviate into one of the two materials. Therefore, in order to fully exploit the advantages of multi-layered structural composites and protective coatings in improving the strength, toughening and surface properties of many engineering components, it becomes necessary to understand more thoroughly the detailed mechanisms by which a crack may grow and propagate along the interface between a porous ductile metal and a stiff substrate.

The near-tip asymptotic fields of a crack steadily growing along a ductile/brittle interface under plane strain conditions have been investigated by several authors. Guo and Keer (1990) and Drugan (1991) studied the problem of interface crack propagation between an elastic–perfectly plastic material obeying the von Mises yield condition and a brittle substrate modeled as rigid, by means of limit analysis theory. Ponte Castañeda and Mataga (1991) extended the analysis to the interface between elastic and ductile materials, the latter being characterized by the J_2-flow theory of plasticity with linear strain hardening. These analyses show that the problem is inherently mixed mode in nature and that, in particular, near the growing crack-tip only two families of solutions are possible. The first one displays a stress field mainly of the tensile type (mode I-like), while the other one results prevalently of shear type (mode II-like). Moreover, if the Dugdale elastic parameter is different from zero, a solution in variable-separable form only exists if the hardening coefficient is lower than a critical value (Ponte Castañeda and Mataga, 1991). For higher hardening values the asymptotic stress fields may display a complex singularity, in agreement with the problem of a crack at the interface between a linear elastic materials and a rigid substrate (Williams, 1959). Later, Bose et al. (1999) extended the investigation to the full-field problem by using the finite element method. These authors found that for the small scale yielding problem the near-tip mode mix is, to a large extent, independent of the external applied elastic fields and, in particular, for a wide range of applied external loadings the mode I-like stress fields prevail at crack-tip, even when the remote loading has a significant mode II component. Moreover, experimental results (Liechiti and Chai, 1991, 1992) revealed that the dimension of the plastic zone and the toughness of the shear-like mode are greater than those relevant to the tensile-like mode. It is worth noting that an increase in the plastic zone size implies higher plastic dissipation and thus a reduction in the amount of external work available for the interface separation process, which means an increase in toughness.

The problem of a stationary crack in a homogeneous porous ductile metal was initially addressed by Drugan and Miao (1992) and Miao and Drugan (1993). The investigation was extended by Miao and Drugan (1995) to steady crack propagation and by Radi and Bigoni (1994, 1996) to mixed isotropic/kinematic hardening behavior. All these analyses consider a constant porosity version of the constitutive model developed by Gurson (1977) and later reviewed by Tvergaard (1990), which may describe the mechanical behavior of incompletely sintered porous metals and particulate-reinforced metal matrix composites. It should be observed that considering the porosity evolution law provided by the Gurson model

would not be compatible with the representation of the crack-tip fields in variable-separable form. However, the porosity may be reasonably assumed constant out of the very near crack-tip zone, where micro-inhomogeneities, cavitation and finite deformation effects dominate. This assumption yields to a constitutive model simple enough to allow us to perform an asymptotic analysis of the crack-tip fields, in order to investigate the influence of porosity on interface crack propagation. On the contrary, if nucleation and growth of voids are taken into account, the determination of the crack-tip fields may require finite element investigations, as those performed by Aoki et al. (1992). In any case, the effects of the nucleation and growth of the pores are expected to influence the higher order terms of the overall solutions.

The objective of the present work is to study the steady-state crack propagation along the interface between a porous ductile material and a brittle substrate, which is modeled as rigid and perfectly bounded to the elastic–plastic material. The constitutive description of the ductile material is defined in Section 2 by the Gurson model in which constant and uniform porosity distribution is assumed. The problem of crack propagation along the interface between a rigid substrate and a porous ductile material displaying linear isotropic hardening is considered in Section 3 by following the approach previously employed by Radi and Bigoni (1994, 1996) for the analysis of crack growth in homogeneous porous ductile media. The case of elastic–perfectly plastic behavior is then examined in Section 4 by taking advantage of the asymptotic analysis developed by Miao and Drugan (1995) for crack propagation in porous ductile metals under mode I loading conditions. In both Sections 3 and 4, an asymptotic analysis of the crack-tip fields is carried out in order to obtain detailed information on the local stress and deformation fields, and thus on the toughening mechanisms associated with the interface. In agreement with the results obtained by Ponte Castañeda and Mataga (1991) for fully dense materials, two distinct kinds of solution are found, corresponding to mainly tensile or shear crack-tip stress fields, respectively. However, due to the higher hydrostatic stress component, the effect of porosity is more pronounced for the tensile solution, rather than for the shear solution. The results obtained in the present work elucidate the effects of the constitutive parameters on the crack-tip fields, as well as the role played by porosity in the stability of crack propagation and in the occurrence of kinking.

Finally, it must be noted that the results obtained in Section 3 approach those derived through limit analysis theory in Section 4 as the hardening modulus tends to vanish. Moreover, for vanishing small porosities the ductile material coincides with the fully dense matrix and the results obtained by the present formulation recover those reported by Ponte Castañeda and Mataga (1991) for linear isotropic hardening, or by Guo and Keer (1990) and Drugan (1991) for elastic–perfectly plastic behavior.

2. Constitutive equations

Reference is made to the Gurson model of elastic–plastic solids containing spherical voids (Gurson, 1977). The model is based on a yield condition of the form

$$f(\boldsymbol{\sigma}, \sigma_{\mathrm{m}}) = \frac{3|\mathrm{dev}\,\boldsymbol{\sigma}|^2}{2\sigma_{\mathrm{m}}^2} + 2\phi\cosh\left(\frac{\mathrm{tr}\,\boldsymbol{\sigma}}{2\sigma_{\mathrm{m}}}\right) - (1+\phi^2) = 0, \tag{1}$$

where ϕ is the volume fraction of voids, $\boldsymbol{\sigma}$ is the average macroscopic stress tensor and the internal variable σ_{m} denotes the current yield stress of the matrix. Moreover, $\mathrm{dev}\,\boldsymbol{\sigma}$ and $\mathrm{tr}\,\boldsymbol{\sigma}$ denote the deviatoric part and the trace of $\boldsymbol{\sigma}$, respectively. Since the growth and nucleation of voids has been neglected, the void volume fraction ϕ is assumed constant, as done also by Miao and Drugan (1995) and by Radi and Bigoni (1994, 1996), so that the condition of associated plastic flow law for the matrix material implies an associated plastic flow law for the macroscopic porous material. Therefore, the incremental constitutive equations relating the stress rate $\dot{\boldsymbol{\sigma}}$ to the deformation rate $\dot{\boldsymbol{\varepsilon}}$ for linear and isotropic elastic behavior result in:

$$\dot{\boldsymbol{\varepsilon}} = \frac{1}{E}[(1+v)\dot{\boldsymbol{\sigma}} - v(\mathrm{tr}\,\dot{\boldsymbol{\sigma}})\mathbf{I}] + \Lambda\mathbf{Q}, \tag{2}$$

where E and v are the elastic Young modulus and Poisson ratio of the matrix material, respectively, and $\mathbf{Q}$ is a second order tensor proportional to the gradient of the yield function (1), namely:

$$\mathbf{Q} = \frac{\sigma_{\mathrm{m}}}{2}\frac{\partial f}{\partial \boldsymbol{\sigma}} = \frac{3}{2\sigma_{\mathrm{m}}}\mathrm{dev}\,\boldsymbol{\sigma} + \frac{\phi}{2}\sinh\left(\frac{\mathrm{tr}\,\boldsymbol{\sigma}}{2\sigma_{\mathrm{m}}}\right)\mathbf{I}. \tag{3}$$

For linear isotropic hardening behavior the non-negative plastic multiplier Λ in Eq. (2) is given by

$$\Lambda = \frac{\langle \mathbf{Q}\cdot\dot{\boldsymbol{\sigma}}\rangle}{H}, \tag{4}$$

where the MacAuley brackets are defined such that $\langle x\rangle = \mathrm{Sup}\{x, 0\}$ for every real value x, and the hardening modulus H of the macroscopic porous material becomes (see Radi and Bigoni, 1994):

$$H = \frac{\alpha E}{(1-\alpha)}\frac{(\mathbf{Q}\cdot\boldsymbol{\sigma})^2}{(1-\phi)\sigma_{\mathrm{m}}^2}, \tag{5}$$

α being a hardening parameter given by the ratio between the tangent modulus in tension E_{t} and the Young modulus E of the matrix material ($0 < \alpha < 1$). Eq. (5) shows that a positive hardening of the matrix material results in a positive hardening modulus H of the porous material.

Finally, it should be observed that, when linear hardening behavior is considered, the rate of growth of the yield surface, measured by $\dot{\sigma}_{\mathrm{m}}$, results in:

$$\dot{\sigma}_{\mathrm{m}} = \frac{\langle \mathbf{Q}\cdot\dot{\boldsymbol{\sigma}}\rangle}{\mathbf{Q}\cdot\boldsymbol{\sigma}}\sigma_{\mathrm{m}}, \tag{6}$$

whereas for perfectly plastic behavior the yield stress is constant and the plastic multiplier Λ becomes an undefined scalar function to be determined by using the yield condition (1).

In the following, it will be assumed that the incremental constitutive equations (2) and (6) hold when the stress state satisfies the yield condition (1), whereas linear elastic isotropic behavior is considered during elastic unloading.

3. Formulation of the linear hardening problem

The problem of a plane crack propagating at constant velocity c along a rectilinear interface between a porous ductile medium displaying linear isotropic hardening and a rigid substrate is firstly considered (Fig. 1). A cylindrical co-ordinate system (r, ϑ, x_3) moving with the crack-tip towards the $\vartheta = 0$ direction is considered, being the x_3-axis along the straight crack front. The mechanical behavior of the elastic–plastic material is described by the rate constitutive laws (2) and (6), which allow for considering elastic unloading sectors appearing in the proximity of the crack-tip during crack propagation.

The steady-state condition yields the following time derivative rule for any scalar function φ:

$$\dot{\varphi} = \frac{c}{r}(\varphi_{,\vartheta}\sin\vartheta - r\,\varphi_{,r}\cos\vartheta). \tag{7}$$

The conditions of kinematics compatibility for infinitesimal deformations and quasi-static equilibrium are

$$\dot{\boldsymbol{\varepsilon}} = \frac{1}{2}(\nabla\mathbf{v} + \nabla\mathbf{v}^{\mathrm{T}}), \tag{8}$$

$$\mathrm{div}\,\boldsymbol{\sigma} = 0. \tag{9}$$

Moreover, in the present analysis the plane strain condition $\dot{\boldsymbol{\varepsilon}}_{33} = 0$ is also considered.

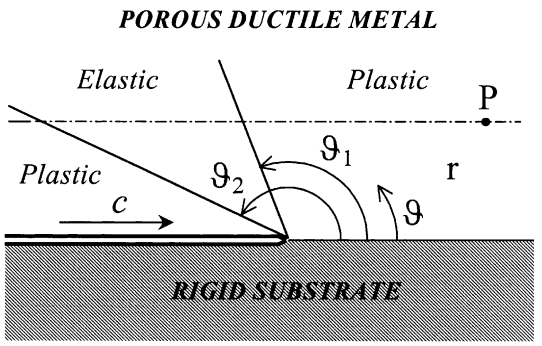

Fig. 1. Cylindrical co-ordinate system centered at the moving interface crack-tip and trajectory of the material point P through plastic and elastic sectors, bounded by angles ϑ_1 and ϑ_2.

Compatibility (8), equilibrium (9) and constitutive incremental equations (2) and (6) form a first order PDEs system, which governs the problem of crack propagation. The solution can be searched in variable-separable form, by considering single term asymptotic expansions of near crack-tip fields. In particular, velocity, stress, and current yield stress fields may be expressed as:

$$\mathbf{v}(r,\vartheta) = -\frac{c}{s}\left(\frac{r}{B}\right)^{s}\mathbf{w}(\vartheta), \tag{10a}$$

$$\boldsymbol{\sigma}(r,\vartheta) = E\left(\frac{r}{B}\right)^{s}\mathbf{T}(\vartheta), \tag{10b}$$

$$\sigma_{\mathrm{m}}(r,\vartheta) = E\left(\frac{r}{B}\right)^{s}T_{\mathrm{m}}(\vartheta), \tag{10c}$$

where the (negative) exponent s is the strength of the stress singularity, and B is a characteristic dimension of the plastic zone, which remains undetermined by the asymptotic analysis, since the lower order problem is homogeneous. Nevertheless, the amplitude of the asymptotic fields can be estimated by a matching procedure with the findings of a full-field numerical analysis, as, for instance, the finite element investigations performed by Aoki et al. (1992).

For the sake of clearness as well as for a proper definition of the plastic reloading condition, the current yield stress σ_{m} in Eq. (10c) has been explicitly assumed as an additional unknown function, instead of deriving it from the yield condition (1) as an implicit function of the stress $\boldsymbol{\sigma}$.

The introduction of the asymptotic stress fields representation (10b) into equilibrium equations (9), yields the following two ODEs:

$$T_{r\vartheta,\vartheta} = -(1+s)T_{rr} + T_{\vartheta\vartheta}, \tag{11a}$$

$$T_{\vartheta\vartheta,\vartheta} = -(2+s)T_{r\vartheta}. \tag{11b}$$

As follows from Eqs. (7),(8) and (10a)–(10c), the rates of the fields $\boldsymbol{\varepsilon}, \boldsymbol{\sigma}$ and σ_{m} may be written as:

$$\begin{aligned}
\dot{\boldsymbol{\varepsilon}} &= -\frac{c}{sr}\left(\frac{r}{B}\right)^{s}\mathbf{D}(\vartheta),\\
\dot{\boldsymbol{\sigma}} &= \frac{cE}{r}\left(\frac{r}{B}\right)^{s}\boldsymbol{\Sigma}(\vartheta),\\
\dot{\sigma}_{\mathrm{m}} &= \frac{cE}{r}\left(\frac{r}{B}\right)^{s}\Sigma_{\mathrm{m}}(\vartheta),
\end{aligned} \tag{12}$$

where the cylindrical components of $\mathbf{D}$ result in:

$$\begin{aligned} D_{rr} &= sw_r, \\ D_{\vartheta\vartheta} &= w_{\vartheta,\vartheta} + w_r, \\ D_{r\vartheta} &= \tfrac{1}{2}[w_{r,\vartheta} - (1-s)w_\vartheta], \end{aligned} \tag{13}$$

and the cylindrical components of $\mathbf{\Sigma}$ and the current yield stress Σ_{m} are given by

$$\Sigma_{r\vartheta} = -s(T_{rr}\sin\vartheta + T_{r\vartheta}\cos\vartheta), \tag{14a}$$

$$\Sigma_{\vartheta\vartheta} = -s(T_{r\vartheta}\sin\vartheta + T_{\vartheta\vartheta}\cos\vartheta), \tag{14b}$$

$$\Sigma_{rr} = (T_{rr,\vartheta} - 2T_{r\vartheta})\sin\vartheta - sT_{rr}\cos\vartheta, \tag{14c}$$

$$\Sigma_{33} = T_{33,\vartheta}\sin\vartheta - s\ T_{33}\cos\vartheta, \tag{14d}$$

$$\Sigma_{\mathrm{m}} = T_{\mathrm{m},\vartheta}\sin\vartheta - s\ T_{\mathrm{m}}\cos\vartheta. \tag{14e}$$

It is worth noting that, when the asymptotic stress fields (10b) and (10c) are introduced in Eqs. (1) and (3), the yield function f and its gradient $\mathbf{Q}$ becomes independent of r and may be written in the form:

$$f(\mathbf{T}, T_{\mathrm{m}}) = \frac{3|\mathrm{dev}\,\mathbf{T}|^2}{2T_{\mathrm{m}}^2} + 2\phi\cosh\left(\frac{\mathrm{tr}\,\mathbf{T}}{2T_{\mathrm{m}}}\right) - (1+\phi^2) = 0, \tag{15}$$

$$\mathbf{Q} = \frac{3}{2T_{\mathrm{m}}}\mathrm{dev}\,\mathbf{T} + \frac{\phi}{2}\sinh\left(\frac{\mathrm{tr}\,\mathbf{T}}{2T_{\mathrm{m}}}\right)\mathbf{I}. \tag{16}$$

As a consequence of the stress field representations (10a)–(10c) and (12), the dimensionless hardening modulus of the porous material $h = H/E$ becomes:

$$h = \frac{\alpha}{(1-\alpha)}\frac{(\mathbf{Q}\cdot\mathbf{T})^2}{(1-\phi)T_{\mathrm{m}}^2}. \tag{17}$$

By substituting the asymptotic fields (10a)–(10c) and their rates (12) into the incremental constitutive relations (2)–(6) and taking into account (13), the following system of five equations is obtained:

$$w_{r,\vartheta} = (1-s)w_\vartheta - 2s[(1+\nu)\Sigma_{r\vartheta} + \lambda Q_{r\vartheta}], \tag{18a}$$

$$w_{\vartheta,\vartheta} = -w_r - s[\Sigma_{\vartheta\vartheta} - \nu(\Sigma_{rr} + \Sigma_{33}) + \lambda Q_{\vartheta\vartheta}], \tag{18b}$$

$$\Sigma_{rr} - \nu(\Sigma_{\vartheta\vartheta} + \Sigma_{33}) + \lambda Q_{rr} + w_r = 0, \tag{18c}$$

$$\Sigma_{33} - \nu(\Sigma_{\vartheta\vartheta} + \Sigma_{rr}) + \lambda Q_{33} = 0, \tag{18d}$$

$$T_{\mathrm{m},\vartheta}\sin\vartheta = \left(s\cos\vartheta + \frac{\lambda h}{\mathbf{Q}\cdot\mathbf{T}}\right)T_{\mathrm{m}}, \tag{18e}$$

where λ is given by

$$\lambda = \frac{1}{h}\langle\mathbf{Q}\cdot\mathbf{\Sigma}\rangle, \tag{19}$$

if the stress fields meet the yield condition (15), else $\lambda = 0$. During elastic unloading λ is set equal to 0 and, thus, the constitutive relations (18a)–(18d) reduce to the incremental equations of linear isotropic elasticity and equation (18e) becomes equivalent to the condition $\dot{\sigma}_{\mathrm{m}} = 0$.

Eqs. (18a)–(18e) together with equilibrium equations (11a) and (11b), result in seven non-linear homogeneous first order ODEs, which do not admit a closed-form analytical solution for the seven unknown angular functions w_r, w_ϑ, $T_{r\vartheta}$, T_{rr}, $T_{\vartheta\vartheta}$, T_{33} and T_{m}. In order to employ a numerical integration procedure, the ODEs (18a)–(18e) should be transformed in explicit form. In particular, from Eqs. (18c) and (18d) the following two equations may be derived:

$$\begin{aligned}(h+\mathrm{Q}_{rr}^2)\Sigma_{rr}-(vh-\mathrm{Q}_{rr}Q_{33})\Sigma_{33}&=-w_r h+(vh-Q_{rr}Q_{\vartheta\vartheta})\Sigma_{\vartheta\vartheta}-2Q_{rr}Q_{r\vartheta}\Sigma_{r\vartheta},\\(vh-Q_{rr}Q_{33})\Sigma_{rr}-(h+Q_{33}^2)\Sigma_{33}&=2Q_{33}Q_{r\vartheta}\Sigma_{r\vartheta}-(vh-Q_{33}Q_{\vartheta\vartheta})\Sigma_{\vartheta\vartheta}.\end{aligned} \tag{20}$$

Eqs. (14a) and (14b) make clear that $\Sigma_{r\vartheta}$ and $\Sigma_{\vartheta\vartheta}$ do not depend on the derivatives of the unknown functions, and so the right-hand sides of Eq. (20). Therefore, Eqs. (20) may be solved for Σ_{rr} and Σ_{33} (see Radi and Bigoni, 1994, 1996). Once Σ_{rr} and Σ_{33} are known, the derivatives of the stress components T_{rr} and T_{33} with respect to the angular co-ordinate ϑ may be obtained from Eqs. (14c) and (14d):

$$\begin{aligned}T_{rr,\vartheta}&=2T_{r\vartheta}+(sT_{rr}\cos\vartheta+\Sigma_{rr})/\sin\vartheta,\\T_{33,\vartheta}&=(sT_{33}\cos\vartheta+\Sigma_{33})/\sin\vartheta.\end{aligned} \tag{21}$$

Similarly, the derivative of w_r and w_ϑ can easily be obtained from constitutive relations (18a) and (18b) by using Eq. (19).

Eqs. (11a), (11b), (18a), (18b), (18e) and (21) form the first order ODEs system, which governs the near-tip stress and velocity fields. This system may be written in the explicit form:

$$\mathbf{y}'(\vartheta)=\begin{cases}\mathbf{f}_{\mathrm{p}}(\vartheta,\mathbf{y}(\vartheta),s) & \text{if} \quad f(\mathbf{T},T_{\mathrm{m}})=0 \quad \text{and} \quad \mathbf{Q}\cdot\boldsymbol{\Sigma}>0,\\ \mathbf{f}_{\mathrm{e}}(\vartheta,\mathbf{y}(\vartheta),s) & \text{if} \quad f(\mathbf{T},T_{\mathrm{m}})<0 \quad \text{or} \quad f(\mathbf{T},T_{\mathrm{m}})=0 \ \text{and} \ \mathbf{Q}\cdot\boldsymbol{\Sigma}\leqslant 0,\end{cases} \tag{22}$$

where the vector

$$\mathbf{y}=\{w_r,w_\vartheta,T_{r\vartheta},T_{rr},T_{\vartheta\vartheta},T_{33},T_{\mathrm{m}}\}, \tag{23}$$

collects the unknown velocity and stress functions of the angular co-ordinate ϑ. It is worth noting that the unknown stress and velocity singularity s may be determined as an eigenvalue of the non-linear homogeneous problem (see Bose and Ponte Castañeda, 1992), which also requires a normalization condition.

3.1. Elastic unloading and secondary plastic reloading

Reference is made to a generic material point P at a small distance from the interface (Fig. 1). Under the assumption of small deformations, the trajectory of the point P with respect to the moving crack-tip may be assumed to occur along a straight path parallel to the interface, so that the angular co-ordinate ϑ singles out the position of the material point. As the crack-tip approaches and, then, goes beyond the material point, the point experiences plastic loading, elastic unloading and subsequent plastic reloading. In particular, the material point, initially ahead of the crack-tip, leaves the plastic loading sector at the elastic unloading angle ϑ_1 where the plastic multiplier λ vanishes, namely for:

$$\mathbf{Q}(\vartheta_1)\cdot\boldsymbol{\Sigma}(\vartheta_1)=0. \tag{24}$$

Throughout the elastic unloading sector the plastic multiplier λ vanishes, the rate constitutive laws (18a)–(18d) reduce to the usual linear isotropic elastic relations and the current yield stress σ_{m} of the material point remains constant and equal to the value assumed at the elastic unloading angle ϑ_1. Plastic reloading on crack flanks occurs at the angle ϑ_2 where the material point reaches a stress state lying on the yield surface left at unloading, that is when the following condition holds true:

$$f(\mathbf{T}(\vartheta_2),T_{\mathrm{m}}(\vartheta_2))=0. \tag{25}$$

3.2. Interface boundary conditions and numerical integration procedure

The condition of perfect adherence between the ductile material and the rigid substrate ahead of the crack-tip implies the vanishing of the velocity functions along the interface plane at $\vartheta = 0$, namely:

$$w_\vartheta(0) = w_r(0) = 0, \tag{26}$$

whereas vanishing of tractions must be imposed on the free crack surface at $\vartheta = \pi$:

$$T_{\vartheta\vartheta}(\pi) = T_{r\vartheta}(\pi) = 0. \tag{27}$$

By using boundary conditions (26) and relations (14a)–(14e) evaluated at $\vartheta = 0$, the constitutive equations (18a)–(18d) become:

$$w_{r,\vartheta}(0) = 2s^2(1+\nu)T_{r\vartheta}(0) - 2s\lambda(0)Q_{r\vartheta}(0), \tag{28a}$$

$$w_{\vartheta,\vartheta}(0) = s^2\{T_{\vartheta\vartheta}(0) - \nu[T_{rr}(0) + T_{33}(0)]\} - s\lambda(0)Q_{\vartheta\vartheta}(0), \tag{28b}$$

$$-s\{T_{rr}(0) - \nu[T_{33}(0) + T_{\vartheta\vartheta}(0)]\} + \lambda(0)Q_{rr}(0) = 0, \tag{28c}$$

$$-s\{T_{33}(0) - \nu[T_{rr}(0) + T_{\vartheta\vartheta}(0)]\} + \lambda(0)Q_{33}(0) = 0, \tag{28d}$$

where $\mathbf{Q}(0)$ and $\lambda(0)$ may be evaluated from Eqs. (16) and (19):

$$\mathbf{Q}(0) = \frac{3}{2T_{\mathrm{m}}(0)}\operatorname{dev}\mathbf{T}(0) + \frac{\phi}{2}\sinh\left(\frac{\operatorname{tr}\mathbf{T}(0)}{2T_{\mathrm{m}}(0)}\right)\mathbf{I}, \tag{29}$$

$$\lambda(0) = -s\frac{(1-\alpha)}{\alpha}\frac{(1-\phi)T_{\mathrm{m}}^2(0)}{\mathbf{Q}(0)\cdot\mathbf{T}(0)}. \tag{30}$$

The dot product:

$$\mathbf{Q}(0)\cdot\mathbf{T}(0) = \frac{3}{2T_{\mathrm{m}}(0)}|\operatorname{dev}\mathbf{T}(0)|^2 + \frac{\phi}{2}[\operatorname{tr}\mathbf{T}(0)]\sinh\left(\frac{\operatorname{tr}\mathbf{T}(0)}{2T_{\mathrm{m}}(0)}\right), \tag{31}$$

is always positive, since $\mathbf{T}(0) \neq 0$. It follows that $\lambda(0) > 0$, i.e. along the interface ahead of the crack-tip the ductile material undergoes plastic loading.

By taking the difference between equations (28c) and (28d) it may be found that:

$$\left[\frac{3\lambda(0)}{2T_{\mathrm{m}}(0)} - s(1+\nu)\right][T_{rr}(0) - T_{33}(0)] = 0. \tag{32}$$

Note that for $s < 0$ the term within square brackets in Eq. (32) is always positive. This means that $T_{33}(0) = T_{rr}(0)$ and thus:

$$\operatorname{tr}\mathbf{T}(0) = T_{\vartheta\vartheta}(0) + 2T_{rr}(0), \tag{33}$$

$$|\operatorname{dev}\mathbf{T}(0)|^2 = \tfrac{2}{3}\{[T_{\vartheta\vartheta}(0) - T_{rr}(0)]^2 + 3T_{r\vartheta}(0)^2\}. \tag{34}$$

In order to solve the system of ODEs (22) the Runge–Kutta procedure is used (IMSL subroutine DIVPRK). This approach requires the knowledge of all the components of $\mathbf{y}(0)$. However, the boundary conditions (26) do not specify the stress components at $\vartheta = 0$, and thus, their values should be preliminarily defined. Firstly, the normalization condition $T_{\mathrm{m}}(0) = 1$ is adopted to avoid the trivial solution due to the homogeneous boundary conditions (26) and (27). Then, $T_{r\vartheta}(0)$ is obtained from the yield condition (15), evaluated at $\vartheta = 0$:

$$T_{r\vartheta}(0)^2 = \tfrac{1}{3}\{1 + \phi^2 - 2\phi\cosh[0.5\,T_{\vartheta\vartheta}(0) + T_{rr}(0)] - [T_{\vartheta\vartheta}(0) - T_{rr}(0)]^2\}, \tag{35}$$

which admits two distinct and opposite roots. Moreover, the position $p = T_{rr}(0)/T_{\vartheta\vartheta}(0)$ is made and finally the value of $T_{\vartheta\vartheta}(0)$ is found as an implicit function of p by solving the following non-linear algebraic equation, obtained from the constitutive relations (28c) and (35):

$$1 + \phi^2 - 2\phi\cosh\xi + \phi\xi\sinh\xi + \frac{(1-\phi)(1-\alpha)}{2\alpha[(1-\nu)p-\nu]}\left[(p+0.5)\phi\frac{\sin\xi}{\xi} + p - 1\right] = 0, \tag{36}$$

where $\xi = (p + 0.5)T_{\vartheta\vartheta}(0)$. Eq. (36) admits at least two opposite roots for ξ, which can be numerically detected (IMSL subroutine DZBREN).

The unknown values of s and p are numerically calculated by the following iterative procedure, based on the achievement of the boundary conditions (27). The integration of the ODEs system (22) is initially performed by assuming arbitrary values of p and s. Then, the corresponding values of $T_{rr}(0)$, $T_{\vartheta\vartheta}(0)$ and $T_{r\vartheta}(0)$ are found from Eqs. (35) and (36) and, thus, the components of $\mathbf{y}(0)$ are fully defined, so that the numerical integration procedure may start. On the basis of a check on the values of $T_{\vartheta\vartheta}(\pi)$ and $T_{r\vartheta}(\pi)$, new improved predictions are obtained for the shooting parameters p and s by employing a modified Powell hybrid method (IMSL subroutine DNEQNF), and the process is iterated until both $T_{\vartheta\vartheta}(\pi)$ and $T_{r\vartheta}(\pi)$ becomes sufficiently close to zero as required by Eq. (27). Finally, all the fields are normalized through the condition $T_{\mathrm{m}}(\vartheta_1) = 1$. Since the asymptotic fields are defined within an amplitude factor, the sign of the normalized solution is chosen so that the velocity fields correspond to interface crack opening. In particular, the sign of $T_{r\vartheta}(0)$ and ξ obtained from Eqs. (35) and (36) is selected so that the velocity component $w_\vartheta(\pi)$ results to be negative or null, in order to avoid interface crack closure.

3.3. Results for the linear hardening problem

Two distinct kinds of solution have been found with slightly different values of the stress singularity and very different, but fixed, mixities of the local crack-tip fields, corresponding to predominantly tensile or shear stress field. Therefore, the discrete near-tip mode mix turns out to be independent of the remote mode mix, as already found by Ponte Castañeda and Mataga (1991) for fully dense ductile material ($\phi = 0$). In the present analysis the solution can be found in variable-separable form only if the hardening coefficient α is lower than a critical value, which depends on the Poisson coefficient ν through the Dugdale parameter ε. For a rigid/elastic interface the latter is given by:

$$\varepsilon = \frac{1}{2\pi}\ln(3 - 4\nu). \tag{37}$$

As noted by Ponte Castañeda and Mataga (1991), the occurrence of a limit hardening value is consistent with the problem of an interface crack between linear elastic materials solved by Williams (1959), which found a complex stress singularity of the form $s = -0.5 + \mathrm{i}\varepsilon$. If the material is elastically incompressible, namely for $\nu = 0.5$, the Dugdale parameter vanishes and the solution can be found for every value of α ranging between 0 and 1. All the results reported in the following have been obtained for the value $\nu = 0.3$, which corresponds to a critical value of α close to 0.275. Note that the existence of other solutions different from those obtained from the variable-separable procedure, could be detected by a full field numerical analysis. However, finite element investigations performed by Bose et al. (1999) for vanishing porosity ($\phi = 0$) confirmed that the near-tip stress state is variable separable of the power singular type and its mode mix is independent of the outer applied mode mix, as also predicted by the asymptotic analysis developed by Ponte Castañeda and Mataga (1991). Analogous results are expected to occur for porous ductile metals.

The effects of porosity on the stress singularity s and on elastic unloading ϑ_1 and plastic reloading ϑ_2 angles are outlined in Figs. 2–4 for both tensile and shear solutions and for two distinct values of the linear

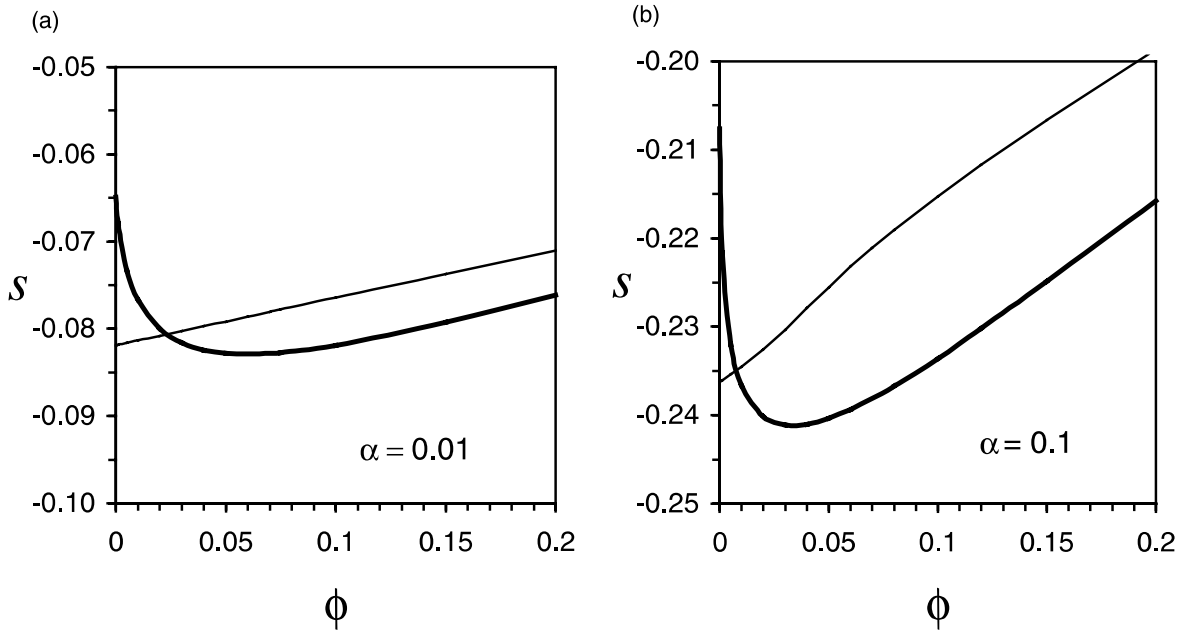

Fig. 2. Strength of the stress singularity s under tensile (bold curve) and shear (solid curve) modes, for $\nu = 0.3$ and two values of α.

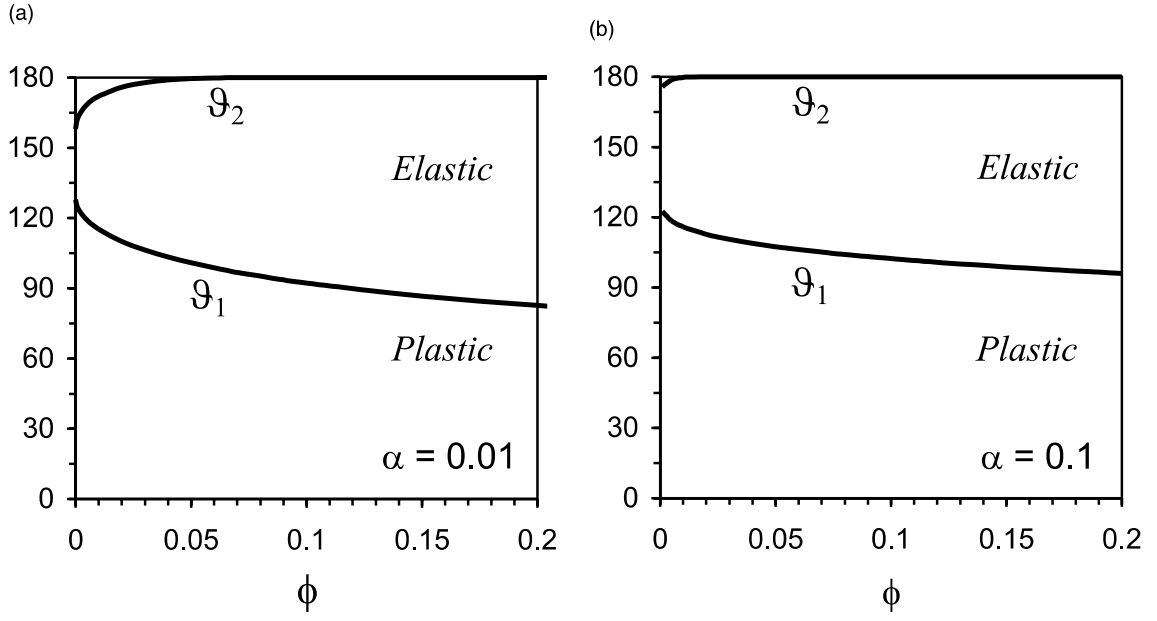

Fig. 3. Elastic unloading ϑ_1 and plastic reloading ϑ_2 angles as functions of porosity for tensile solution, $\nu = 0.3$ and two values of α.

hardening parameter, namely $\alpha = 0.01$ and 0.1. The results presented in Fig. 2 show that for low porosity (Fig. 2a) the strength of the stress singularity, given by the absolute value of s, turns out to be greater for the

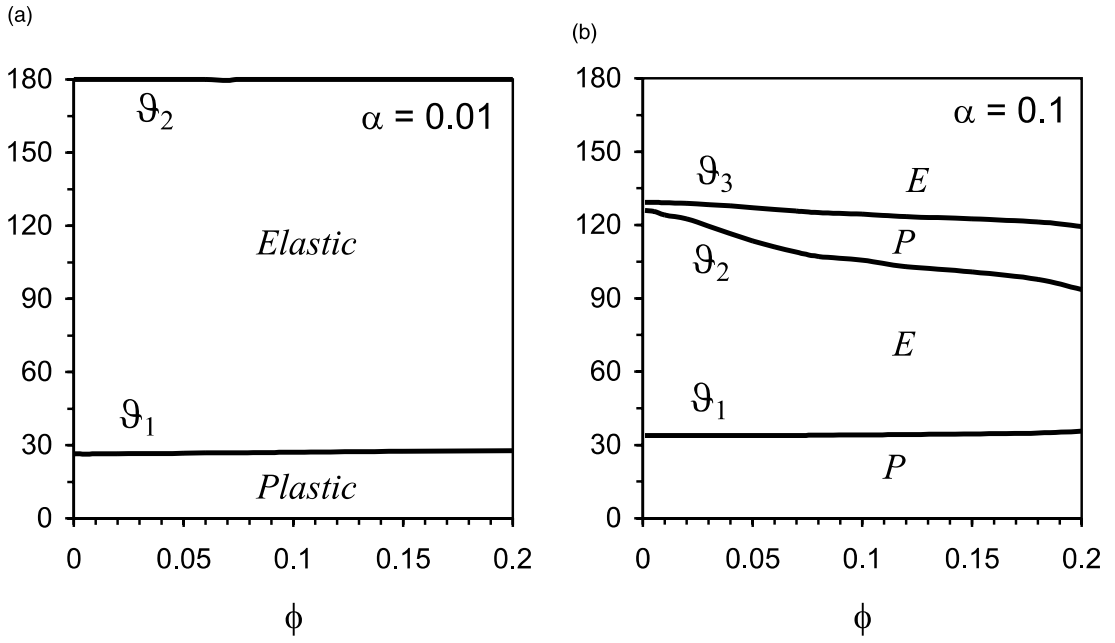

Fig. 4. Elastic unloading ϑ_1 and ϑ_3 and plastic reloading ϑ_2 angles as functions of porosity for shear solution, $\nu = 0.3$ and two values of α.

shear solution than for the tensile solution. However, as the porosity increases (Fig. 2b), the singularity of the tensile mode rapidly increases with respect to the case of fully dense material ($\phi = 0$), whereas the singularity of the shear mode decreases almost linearly and, for high porosity, becomes lower than singularity of the tensile mode.

It should be observed that the decrease in the values of the stress singularity s from the elastic case ($s = -0.5$) to the elastic–perfectly plastic case ($s = 0$) corresponds to a more stable crack propagation. This is due to the plastic dissipation that occurs in the plastic zone surrounding the crack-tip, which causes a reduction in the amount of external work available for the interface separation process. Conversely, an increase in singularity generally reveals instability of the crack propagation (Radi and Bigoni, 1996). It can then be inferred that for low values of porosity the shear mode may be unstable and may be regarded as a transitory state towards a more stable state of near-tip tension, as already observed in the small scale yielding analysis performed by Bose et al. (1999) for $\phi = 0$. On the contrary, the tensile mode may be unstable for high values of porosity.

From Fig. 3 it may be noted that in tensile mode the size of the elastic unloading sector in proximity of the crack-tip enlarges as the porosity increases, so that the plastic deformation tends to concentrate ahead of the crack-tip. As already observed by Radi and Bigoni (1994, 1996), Fig. 4 shows that porosity does not significantly affect the extension of elastic and plastic sectors in shear solution, with the exception of a secondary plastic loading sector, which arises within the elastic unloading sector for high hardening values (see Fig. 4b). Fig. 4 also show that plastic reloading at crack flank ($\vartheta = \vartheta_2$) only occurs for small values of the hardening parameter α, as already found by Ponte Castañeda and Mataga (1991). Moreover, for $\phi = 0$ the results of Figs. 2–4 coincide with the findings of Ponte Castañeda and Mataga (1991) obtained for a rigid substrate ($\beta = 0$) and the same values of α.

The angular variations of the asymptotic stress and velocity fields in tensile mode are plotted in Fig. 5 for a low hardening coefficient ($\alpha = 0.01$) and for two distinct values of porosity, namely $\phi = 0.001$ and 0.1.

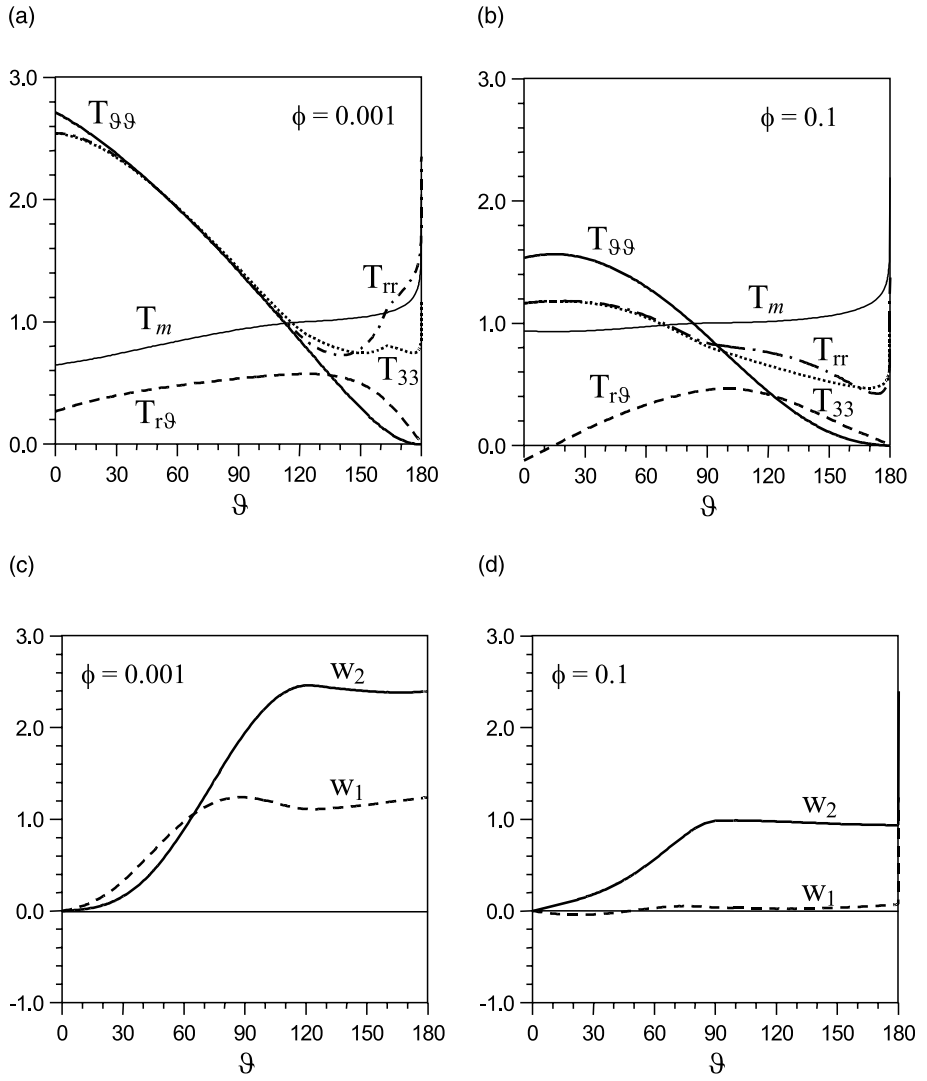

Fig. 5. Angular variations of the stress (a, b) and velocity (c, d) fields near crack-tip under tensile mode, for $\nu = 0.3$, $\alpha = 0.01$ and two distinct values of the porosity ϕ.

Fig. 5a shows that for low values of porosity the tensile stress field ahead of the crack-tip is characterized by large stress triaxiality in the ductile material. In particular, the hydrostatic stress component ahead of the crack-tip exceeds more than three times the current yield stress. From Fig. 5b it may be inferred that the main effects of an increase in the porosity is a lowering of the mean stress, together with a decrease of the shear stress component $T_{r\vartheta}$, which becomes negative along the interface line at $\vartheta = 0$. Correspondingly, in the tensile solution the location of the maximum hoop stress $T_{\vartheta\vartheta}$ deviates from the interface line ahead of the crack-tip towards the porous ductile material. Precisely, the maximum of $T_{\vartheta\vartheta}$ is attained where the shear stress vanishes, as it follows from Eq. (11b). This occurrence may cause possible kinking of the fracture trajectory, so that the interfacial toughness may significantly increase. The stress fields for low hardening

coefficient ($\alpha = 0.01$), reported in Figs. 5a and b, are expected to approach the elastic–perfectly plastic solution. In this case, the near-tip stress fields should display a centered-fan plastic sector starting from the rigid interface almost to the elastic unloading angle ϑ_1, as already found by Guo and Keer (1990), Drugan (1991) and Ponte Castañeda and Mataga (1991) for fully dense ductile material obeying the von Mises yield condition. The corresponding angular variations of the Cartesian components of velocity are shown in Figs. 5c and d. These plots show that the velocity components increase in the plastic loading sector ahead of the crack-tip and then remain almost constant in the crack wake. Moreover, the value of the velocity component w_2 at $\vartheta = \pi$ is positive for all the reported results, thus implying crack opening.

Stress and velocity asymptotic fields for shear mode and low hardening coefficient ($\alpha = 0.01$) are plotted in Fig. 6 for two values of porosity, namely $\phi = 0.001$ and 0.1. The stress fields reported in Figs. 6a and b display positive, but very low, mean stress at $\vartheta = 0$, thus resulting approximately in a mode II solution.

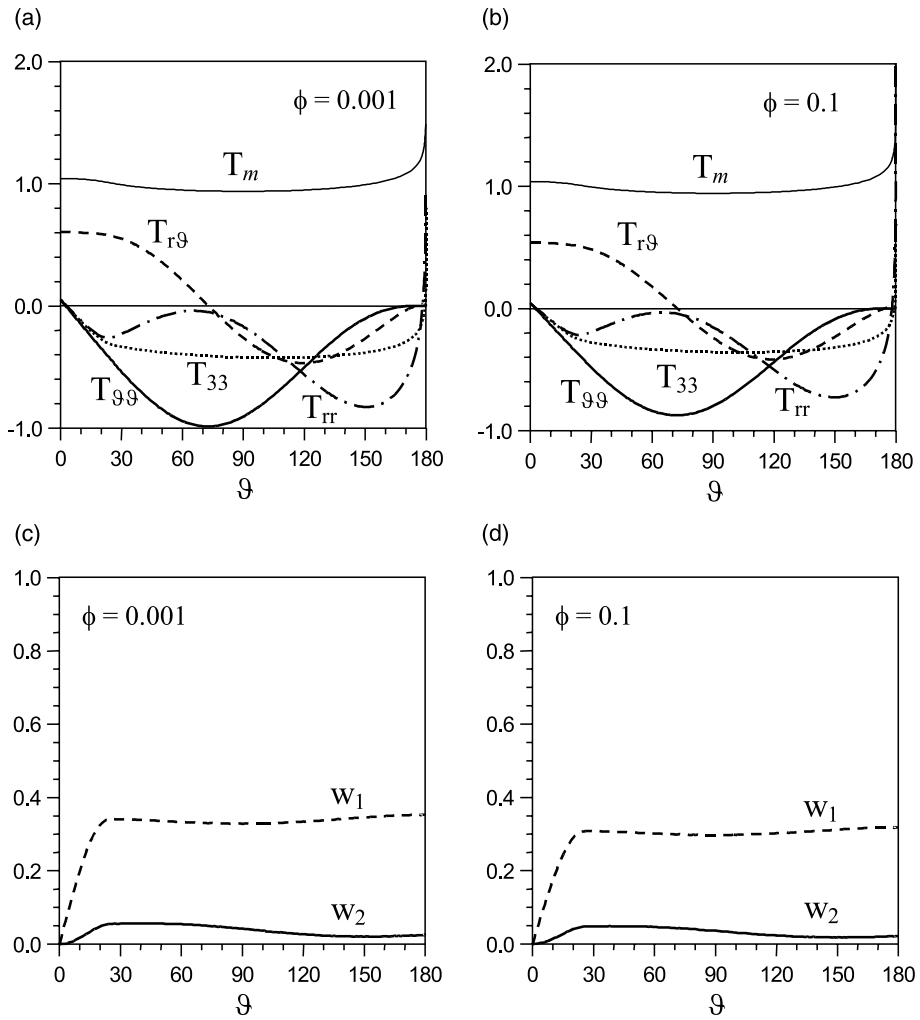

Fig. 6. Angular variations of the stress (a, b) and velocity (c, d) fields near crack-tip under shear mode, for $\nu = 0.3$, $\alpha = 0.01$ and two distinct values of the porosity ϕ.

A comparison between Figs. 5 and 6 points out that the porosity strongly influences the stress fields of the tensile mode while producing modest effects on the shear mode, which is a consequence of the different hydrostatic stress level. Figs. 6a and b also show that, in the limit case of vanishing hardening, a centered-fan plastic sector seems to develop ahead of the crack-tip for the shear solution too.

The stress and velocity fields for tensile mode and high hardening coefficient ($\alpha = 0.1$) are reported in Fig. 7 for low ($\phi = 0.001$) and high ($\phi = 0.1$) porosity. These results are roughly similar to those obtained for the low hardening case plotted in Fig. 5 except that the shear stress component $T_{r\vartheta}$ at $\vartheta = 0$ is negative, also for small porosity.

In Fig. 8 the stress and velocity fields for shear mode and $\alpha = 0.1$ are reported. It should be noted that these fields turn out to be opposite in sign with respect to the low hardening case of Fig. 6. In particular,

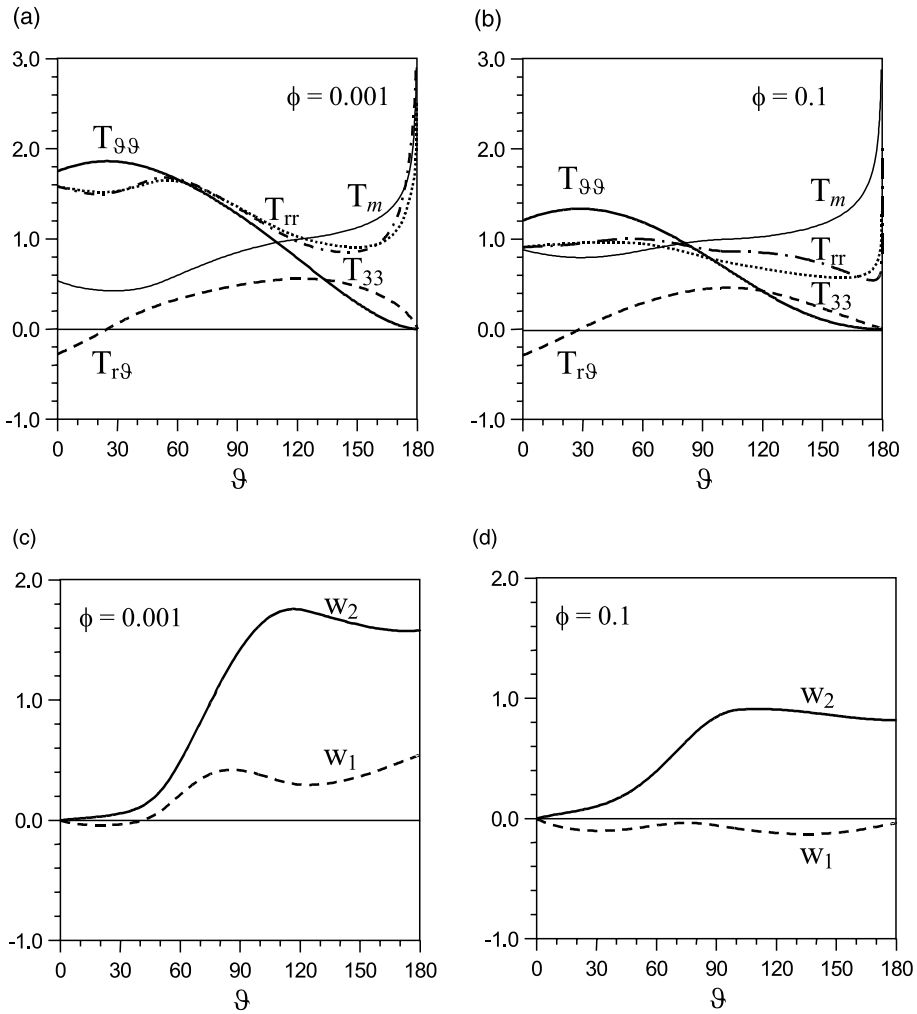

Fig. 7. Angular variations of the stress (a, b) and velocity (c, d) fields near crack-tip under tensile mode, for $\nu = 0.3$, $\alpha = 0.1$ and two distinct values of the porosity ϕ.

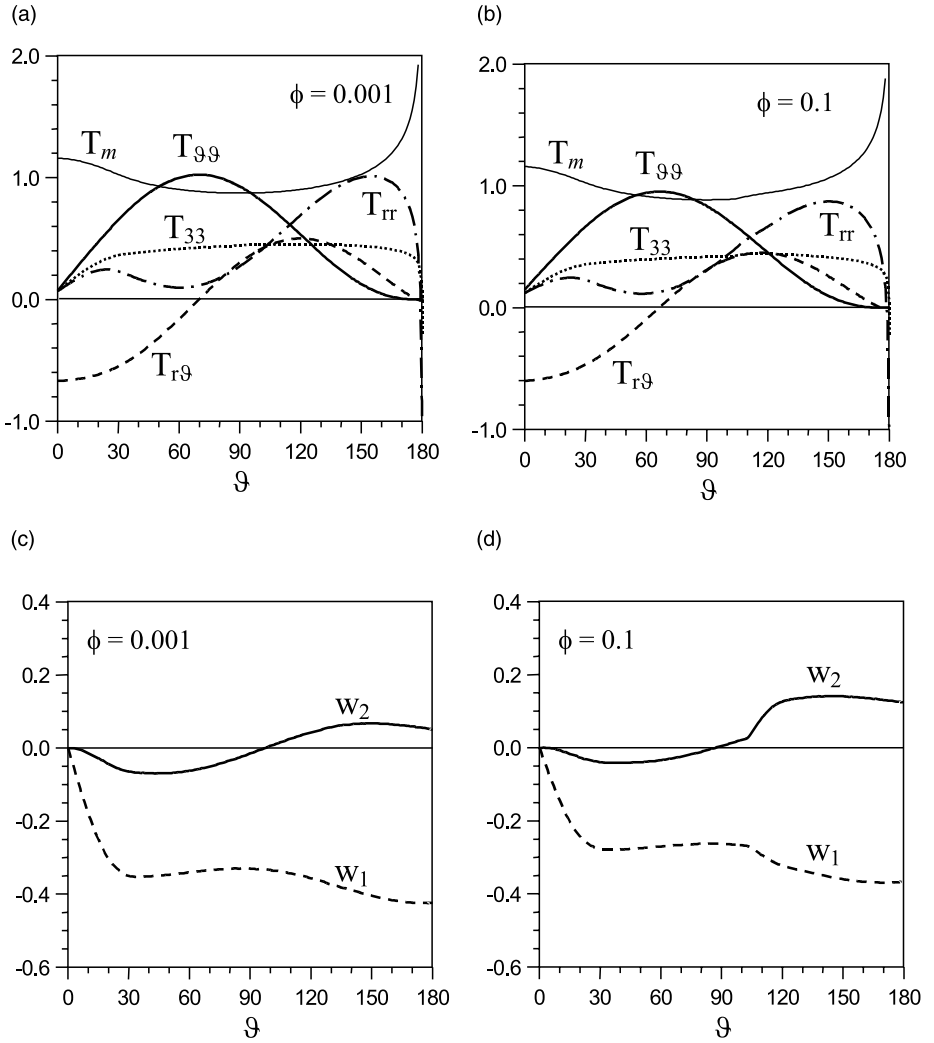

Fig. 8. Angular variations of the stress (a, b) and velocity (c, d) fields near crack-tip under shear mode, for $\nu = 0.3$, $\alpha = 0.1$ and two distinct values of the porosity ϕ.

along the interface line, at $\vartheta = 0$, the shear stress component $T_{r\vartheta}$ is negative, while the hoop stress $T_{\vartheta\vartheta}$ is low but tensile (see Figs. 8a and b), leading thus to crack opening (see the sign of the velocity functions w_2 at $\vartheta = \pi$ in Figs. 8c and d). Note that solutions displaying near-tip fields opposite to those reported in Figs. 5–8 have been rejected since they would imply interface crack closure.

It should be pointed out that linear isotropic hardening may represent an intermediate model between the limit cases of linear elastic and perfectly-plastic constitutive behavior and may adequately account for the dissipation of energy in the plastic zone near the crack-tip, which is responsible for stable crack growth. Nevertheless, the rough model of isotropic hardening may be refined by the introduction of a more realistic mixed isotropic\kinematic hardening behavior, as done by Radi and Bigoni (1994) for crack propagation in homogeneous porous ductile metals.

4. Formulation of the elastic–perfectly plastic problem

As the value of the hardening coefficient α tends to vanish, the elastic–perfectly plastic behavior of the ductile material is approached. In this limit case the current yield stress remains constant, namely $\sigma_m = \sigma_0$, and the stress fields near the crack-tip must be finite as required by the yield condition (1). Therefore, the value of stress singularity s must vanish. Under these conditions, Miao and Drugan (1995) showed that the velocity fields display a logarithmic singularity, which corresponds to the limit behavior of the velocity fields in Eq. (10a) as s approaches 0. Based on this argument the stress and velocity fields may be assumed as:

$$\begin{aligned} &\boldsymbol{\sigma} = \sigma_0 \mathbf{T}(\vartheta), \\ &\mathbf{v} = c\frac{\sigma_0}{E}\mathbf{w}(\vartheta)\ln\frac{B}{r}, \end{aligned} \tag{38}$$

where $\mathbf{T}(\vartheta)$ and $\mathbf{w}(\vartheta)$ are non-dimensional stress and velocity functions of the angular coordinate ϑ, and σ_0 is the yield stress in tension. For perfect plasticity the yield condition (1) reduces to:

$$f(\mathbf{T}) = \frac{3}{2}|\mathrm{dev}\,\mathbf{T}|^2 + 2\phi\cosh\left(\frac{\mathrm{tr}\,\mathbf{T}}{2}\right) - (1+\phi^2) = 0, \tag{39}$$

and the rate constitutive equations (2) may be written as:

$$\dot{\boldsymbol{\varepsilon}} = \sigma_0\left\{\frac{1+\nu}{E}\dot{\mathbf{T}} - \frac{\nu}{E}(\mathrm{tr}\,\dot{\boldsymbol{T}})\mathbf{I} + \Lambda_0\left[3\mathrm{dev}\,\mathbf{T} + 2\phi\cosh\left(\frac{\mathrm{tr}\,\mathbf{T}}{2}\right)\right]\right\}, \tag{40}$$

where the plastic multiplier $\Lambda_0 = \Lambda/(2\sigma_0)$ is a positive scalar function which can be determined by using the yield condition (39).

Miao and Drugan (1995) derived the equations governing the stress and velocity fields for all the admissible types of asymptotic crack-tip sectors in a porous ductile material, under plane strain conditions. They found that the asymptotic near crack-tip fields can be constructed by assembling three different types of plastic sectors, namely generalized centered fan, constant stress and non-singular plastic sectors, together with an elastic unloading sector. However, constant stress plastic sectors do not appear in the asymptotic assembling of near-tip sectors considered here, except for the particular case of $\nu = 0.5$ and $\phi = 0$ analyzed by Guo and Keer (1990), Drugan (1991) and Ponte Castañeda and Mataga (1991). The equations which hold for each of the admissible asymptotic sectors are reported in the following, as derived by Miao and Drugan (1995).

4.1. Generalized centered fan

Within this singular plastically deforming sector, the stress fields are statically determinate and may be found by solving the following first order ODEs system, which do not admit closed-form analytical solutions:

$$T'_{r\vartheta} = T_{\vartheta\vartheta} - T_{rr}, \tag{41a}$$

$$T'_{rr} = \left(1 - \frac{3}{1+\phi\cosh z}\right)T_{r\vartheta}, \tag{41b}$$

$$T'_{\vartheta\vartheta} = -2T_{r\vartheta}, \tag{41c}$$

where

$$z = T_{rr} + \tfrac{1}{2}T_{\vartheta\vartheta}. \tag{42}$$

Within this plastic sector the following condition may be found to hold:

$$T_{33} = T_{rr}. \tag{43}$$

By using Eqs. (41a)–(41c) and the derivative of the yield condition (39) the stress components may be expressed as functions of z, namely:

$$\begin{aligned} &T_{rr} = T_{33} = \tfrac{1}{3}(2z - \phi \sinh z),\\ &T_{\vartheta\vartheta} = \tfrac{2}{3}(z + \phi \sinh z),\\ &T_{r\vartheta} = \pm\sqrt{\tfrac{2}{3}(1+\phi^2) - \tfrac{1}{3}(1+\phi\cosh z)^2}. \end{aligned} \tag{44}$$

The corresponding near-tip velocity fields are defined by the following equations:

$$w_r = -\left[(1-2v)T'_{rr} + T'_{\vartheta\vartheta} + \frac{(T'_{rr})^2}{T'_{rr} + T'_{\vartheta\vartheta}}\right]\sin\vartheta, \tag{45a}$$

$$w'_{\vartheta} = \frac{T'_{r\vartheta}}{2T_{r\vartheta}}(w'_r - w_{\vartheta}) - w_r, \tag{45b}$$

and the plastic multiplier results in:

$$\Lambda_0 = \frac{c}{E}\,\frac{w'_r - w_{\theta}}{6rT_{r\vartheta}}\ln\frac{B}{r}, \tag{46}$$

so that plastic strains in this sector are singular at the crack-tip.

4.2. Non-singular plastic sector

As different from the other sectors, this sector displays finite strains as r approaches zero. The stress fields are not statically determinate and may be found by solving the following first order ODEs system, which also depends on the velocity components w_1 and w_2:

$$\begin{aligned} &T'_{r\vartheta} = T_{\vartheta\vartheta} - T_{rr},\\ &T'_{rr} = -\frac{\hat{S}^2_{33}}{\hat{S}^2_{rr} + \hat{S}^2_{33} + 2v\hat{S}_{rr}\hat{S}_{33}}(w_1\operatorname{cotg}\vartheta + w_2) + 2T_{r\vartheta},\\ &T'_{\vartheta\vartheta} = -2T_{r\vartheta},\\ &T'_{33} = \frac{\hat{S}_{rr}\hat{S}_{33}}{\hat{S}^2_{rr} + \hat{S}^2_{33} + 2v\hat{S}_{rr}\hat{S}_{33}}(w_1\operatorname{cotg}\vartheta + w_2), \end{aligned} \tag{47}$$

where

$$\hat{\mathbf{S}} = \operatorname{dev}\mathbf{T} + \frac{\phi}{3}\sinh\left(\frac{\operatorname{tr}\mathbf{T}}{2}\right)\mathbf{I}. \tag{48}$$

The cartesian components of velocity must be constant, namely

$$w'_1 = 0, \quad w'_2 = 0, \tag{49}$$

and the plastic multiplier has the following expression:

$$\Lambda_0 = -\frac{c}{3Er}\,\frac{\hat{S}_{rr} + v\hat{S}_{33}}{\hat{S}^2_{rr} + \hat{S}^2_{33} + 2v\hat{S}_{rr}\hat{S}_{33}}(w_1\operatorname{cotg}\vartheta + w_2). \tag{50}$$

4.3. Elastic unloading sector

In near-tip sectors undergoing elastic unloading, the stress fields are defined by the following ODEs

$$\begin{aligned} T'_{r\vartheta} &= T_{\vartheta\vartheta} - T_{rr}, \\ T'_{rr} &= -\frac{1}{1-\nu^2}(w_1 \operatorname{cotg}\vartheta + w_2) + 2T_{r\vartheta}, \\ T'_{\vartheta\vartheta} &= -2T_{r\vartheta}, \\ T'_{33} &= -\frac{\nu}{1-\nu^2}(w_1 \operatorname{cotg}\vartheta + w_2), \end{aligned} \tag{51}$$

Also in this case the cartesian velocity components are constant, being:

$$w'_1 = 0, \quad w'_2 = 0. \tag{52}$$

4.4. Asymptotic assembly of sectors

On the basis of the asymptotic analyses of the crack-tip fields for a crack growing along a brittle/ductile interface (Drugan, 1991; Ponte Castañeda and Mataga, 1991) and for a mode I crack in porous ductile metals (Miao and Drugan, 1995), we seek a solution for the elastic–perfectly plastic problem by taking into account the results obtained in Section 3 for low hardening. In this case the asymptotic crack-tip fields are obtained by assembling together a generalized centered fan sector A ahead of the crack-tip ($0 < \vartheta < \vartheta_0$), a non-singular plastic sector B ($\vartheta_0 < \vartheta < \vartheta_1$), an elastic unloading sector C ($\vartheta_1 < \vartheta < \vartheta_2$), and finally, another non-singular plastic sector D extending to the upper crack face ($\vartheta_2 < \vartheta < \pi$) (see Fig. 9).

The solution is obtained by numerically integrating the field equations relevant to each sector (IMSL subroutine DIVPRK) and imposing full stress and velocity continuity across the mutual border between

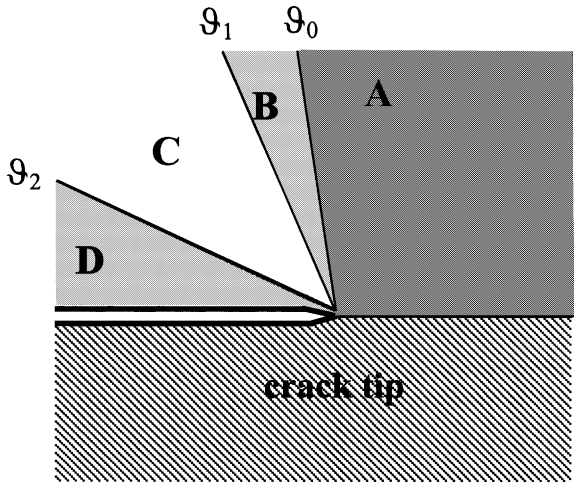

Fig. 9. Assembling of asymptotic sectors near crack-tip for elastic–perfectly plastic behavior of the ductile material: generalized centered-fan plastic sector (A), non-singular plastic sectors (B and D) and elastic unloading sector (C), bounded by angles ϑ_0, ϑ_1 and ϑ_2.

each pair of sectors. Moreover, the vanishing of velocity along the interface line ahead of the crack-tip (26) and the vanishing of tractions on the crack surface (27) must be imposed as boundary conditions.

The values of of $z_0 = z(0)$ and of the angle ϑ_0 are chosen to be the two shooting parameters in the numerical iterative procedure based on the achievement of the boundary conditions (27), in analogy with the procedure followed in Section 3. When z_0 is known, the stress field at $\vartheta = 0$ is fully determined by Eqs. (44), so that the numerical procedure may start. The ODEs system formed by Eqs. (41a)–(41c), (45a) and (45b) is numerically integrated in the generalized centered-fan plastic sector A extending from $\vartheta = 0$ to $\vartheta = \vartheta_0$. Then, the ODEs system (47) is numerically integrated for $\vartheta_0 \leqslant \vartheta \leqslant \vartheta_1$, being the elastic unloading angle ϑ_1 determined by the condition that the plastic multiplier (50) must vanish at the end of the non-singular plastic sector B. The stress fields in the elastic unloading sector C are numerically determined by integrating the ODEs system (51) for $\vartheta_1 \leqslant \vartheta \leqslant \vartheta_2$, where the plastic reloading angle ϑ_2 is defined by requiring that the stress fields at the end of the elastic unloading sector satisfy the yield condition (39). Finally, the stress fields in the non-singular plastic sector D adjacent to the crack surface are determined by integrating the ODEs system (47) for $\vartheta_2 \leqslant \vartheta \leqslant \pi$. As required by Eqs. (49) and (52), the cartesian components of velocity in the non-singular plastic sectors B and D and in the elastic sectors C must be constant and, thus, equal to their values at the end of the generalized centered fan, namely at $\vartheta = \vartheta_0$. By checking the values of $T_{\vartheta\vartheta}(\pi)$ and $T_{r\vartheta}(\pi)$, new improved predictions are obtained for the shooting parameters ϑ_0 and z_0 and the process can be iterated (IMSL subroutine DNEQNF) until $T_{\vartheta\vartheta}(\pi)$ and $T_{r\vartheta}(\pi)$ become sufficiently close to zero, as required by the boundary conditions (27). Moreover, a check on the values of the plastic multiplier Λ_0 is performed in all the plastic sectors in order to ensure that it is always greater than zero.

It should be noted that solutions with continuous stress fields but discontinuous radial velocity fields may also be admissible, as proved by Drugan and Rice (1984) for a general class of elastic–perfectly plastic materials. However, in the present investigation we have looked for solutions with continuous velocity fields only.

4.5. Results for the elastic–perfectly plastic problem

Similarly to the linear hardening problem investigated in Section 3, also in the case of elastic–perfectly plastic behavior, two distinct solutions have been found for every set of material parameters, corresponding to mainly tensile or shear mode. In particular, in order to make clear the effects of porosity the results reported in the following refer to the same value of the Poisson ratio, $\nu = 0.3$, considered in the previous section.

Fig. 10a and 10b display the angular location of sector borders, defined by the angles ϑ_0, ϑ_1 and ϑ_2, as functions of porosity for tensile and shear modes, respectively. The results relevant to the tensile mode in Fig. 10a confirm that an increase in porosity yields an enlargement of the elastic sector and a concentration of plastic deformation ahead of the crack-tip, as also observed for low hardening. Fig. 10b reveals that for the shear solution the porosity produces weak effects on the size of the asymptotic crack-tip sectors. The numerical values of the bordering sector angles ϑ_0, ϑ_1 and ϑ_2 are also reported in Table 1 for different values of porosity.

The angular variation of stress and velocity fields for the tensile mode are plotted in Fig. 11 both for near fully dense ($\phi = 0.001$) and for porous ($\phi = 0.05$) ductile material. From these figures it may be observed that the effects of an increase in porosity mainly consist of a lowering of the mean hydrostatic stress and of the shear stress along the interface line. In particular, for $\phi = 0.05$ the shear stress almost vanishes at $\vartheta = 0$, and thus the crack-tip fields almost result in a pure mode I solution. For higher values of porosity the stress fields display a negative shear stress along the interface together with a shift of the location of the maximum opening stress towards the ductile material. This maximum is attained within the generalized centered-fan

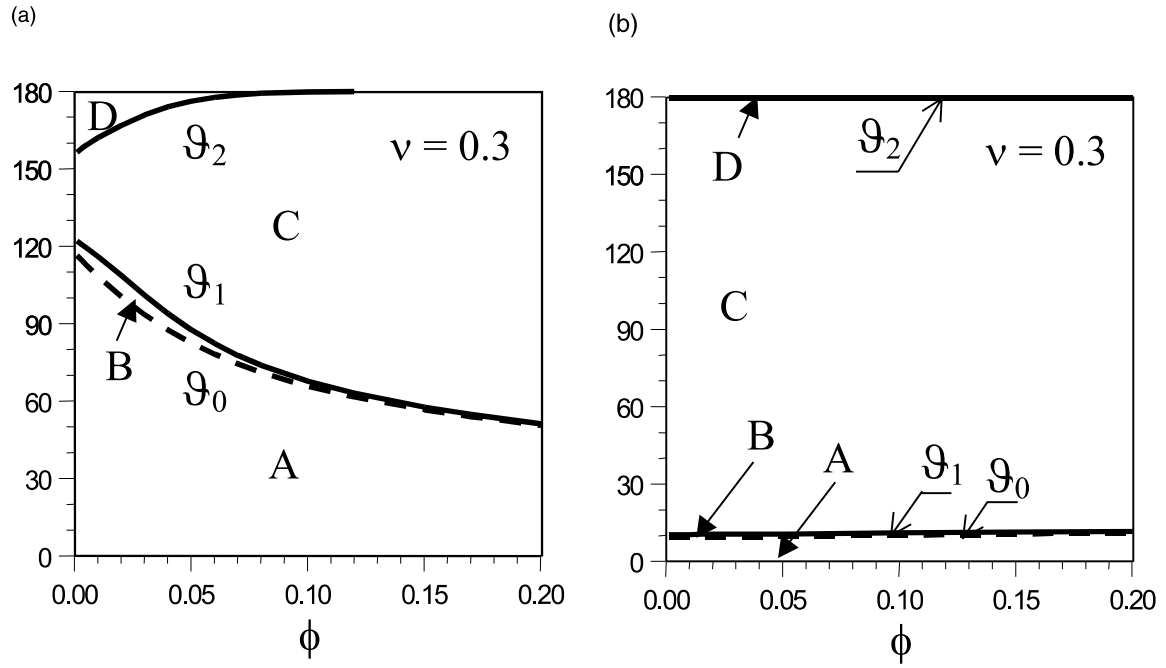

Fig. 10. Angles ϑ_0, ϑ_1 and ϑ_2 as functions of porosity for tensile (a) and (b) shear solutions, for $\nu = 0.3$ and elastic–perfectly plastic behavior of the ductile material.

Table 1
Values of the angles ϑ_0, ϑ_1 and ϑ_2, for $\nu = 0.3$, elastic–perfectly plastic behavior and different values of porosity ϕ, under plane strain conditions both for tensile and shear solutions

ϕ	Tensile mode			Shear mode		
	ϑ_0	ϑ_1	ϑ_2	ϑ_0	ϑ_1	ϑ_2
0.000	117.37	122.81	155.77	9.30	10.44	179.79
0.001	116.37	122.10	156.53	9.30	10.45	179.79
0.005	112.63	119.38	159.19	9.34	10.47	179.79
0.010	108.30	115.96	162.06	9.39	10.50	179.79
0.015	104.21	112.38	164.63	9.43	10.53	179.79
0.020	100.37	108.65	166.96	9.48	10.56	179.79
0.050	82.55	87.59	176.27	9.75	10.73	179.78
0.100	65.75	67.74	179.82	10.20	11.01	179.76
0.150	56.65	57.70	–	10.64	11.30	179.75
0.200	50.58	51.21	–	11.07	11.60	179.73

sector exactly at the same angle ϑ^* of vanishing shear stress, as required by (41c). This occurrence may be observed in Fig. 12a, where the angular variations of the stress fields are plotted for $\phi = 0.15$. Correspondingly, Fig. 12b reveals that the circumferential velocity component w_ϑ attains a peak exactly at the same angle ϑ^* where the shear stress vanishes, as also confirmed by Eq. (45b). The peak for w_ϑ results in a singularity for the opening strain rate

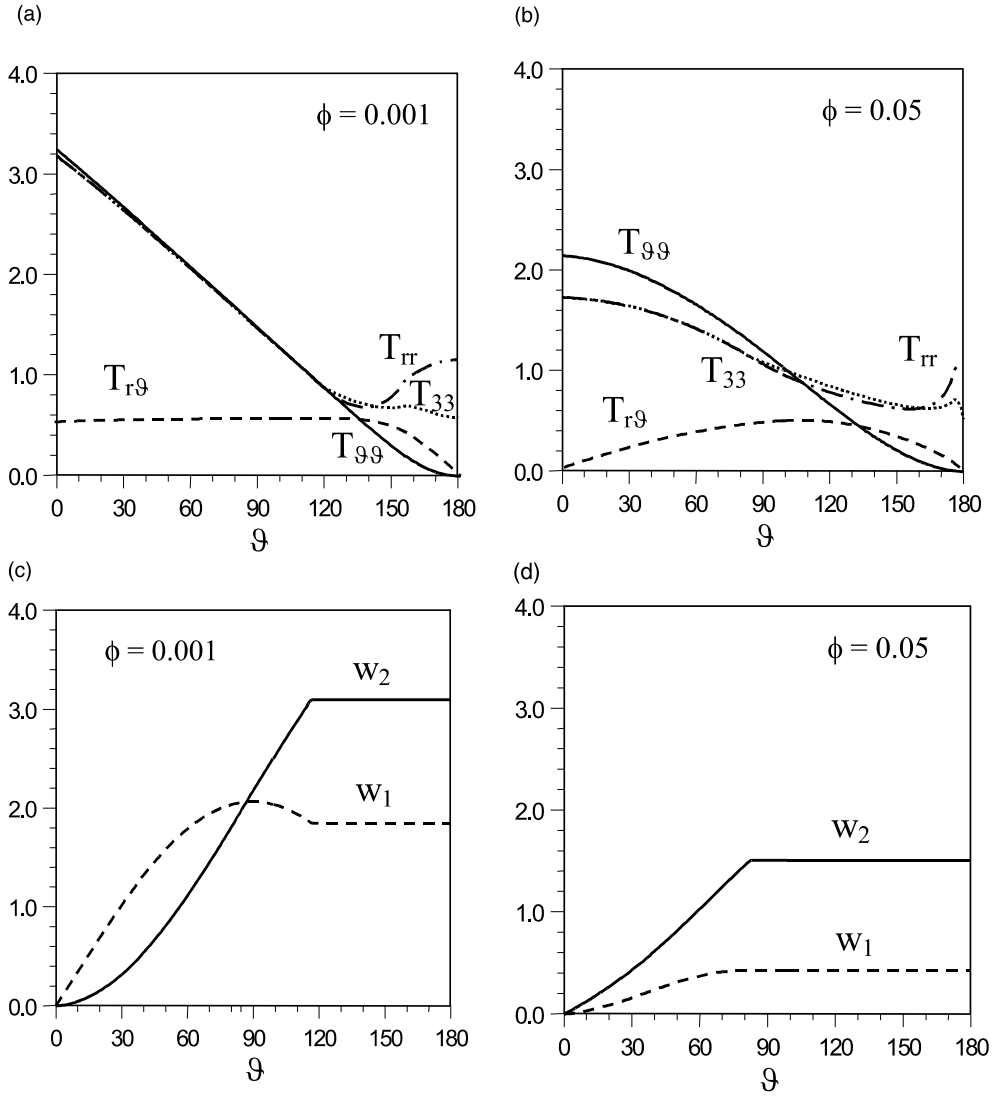

Fig. 11. Angular variations of the stress (a,b) and velocity (c,d) fields near crack-tip under tensile mode for elastic–perfectly plastic behavior, $\nu = 0.3$ and two distinct values of the porosity ϕ.

$$\dot{\varepsilon}_{\vartheta\vartheta} = \frac{1}{r}(v_{\vartheta,\vartheta} + v_r), \tag{53}$$

which jumps from $-\infty$ to $+\infty$ along the radial line defined by $\vartheta = \vartheta^*$. All these occurrences confirm the tendency of the crack trajectory to kink towards the porous ductile material, which may yield an increase in the interface toughness, also due to the roughness of the fracture surface produced by microbranching of the main crack into the ductile material.

As already discussed in Section 3, porosity causes modest variations on shear solution and, thus, the angular variation of the stress and velocity fields for shear mode have been reported only for the value of $\phi = 0.01$ (Fig. 13).

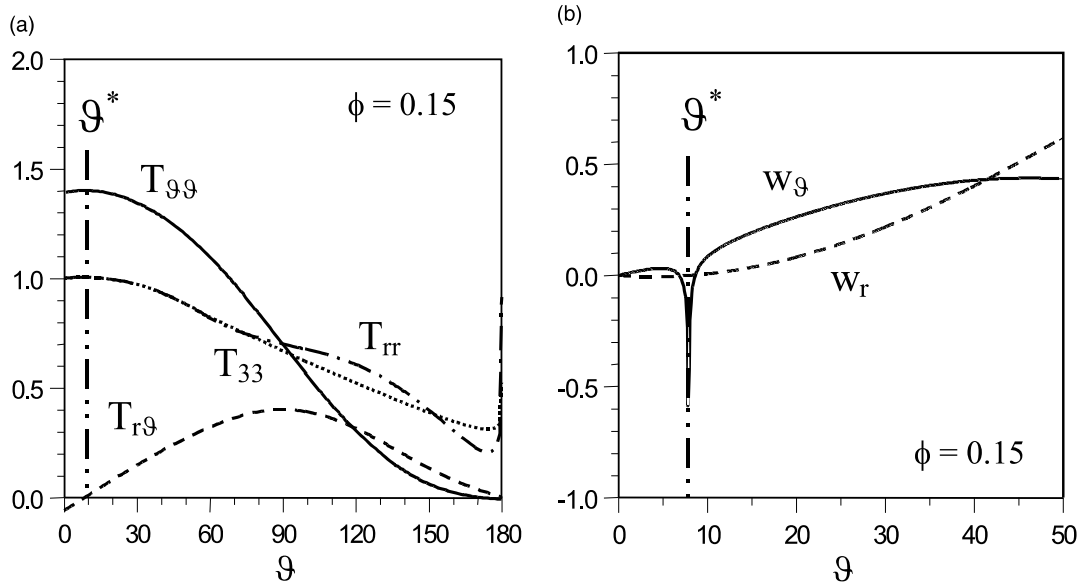

Fig. 12. Angular variations of the stress (a) and velocity (b) fields near crack-tip under tensile mode for elastic–perfectly plastic behavior, $\nu = 0.3$ and $\phi = 0.15$. The cylindrical components of velocity have been plotted just for $0 < \vartheta < 50°$ to point out the discontinuity at $\vartheta = \vartheta^*$.

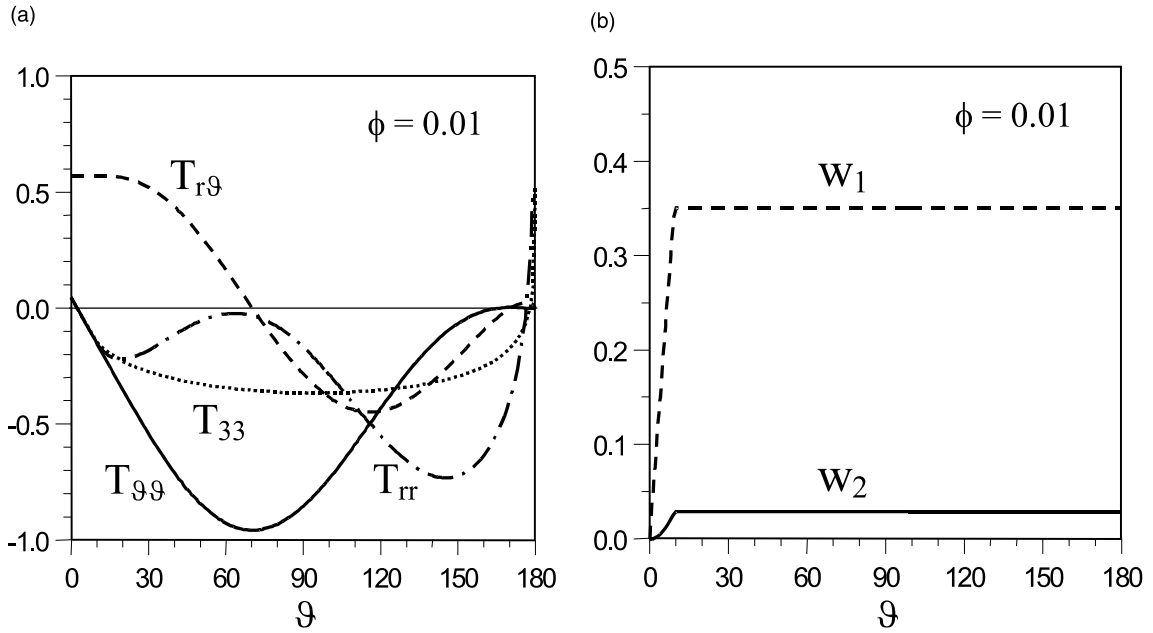

Fig. 13. Angular variations of the stress (a) and velocity (b) fields near crack-tip under shear mode for elastic–perfectly plastic behavior, $\nu = 0.3$ and $\phi = 0.01$.

5. Conclusions

The performed near-tip asymptotic analysis predicts, rather accurately, the stress singularity and the near-tip mode mix for a crack between a porous ductile metal and a stiffer substrate. It gives useful predictions about the tendency for crack kinking as well as about the interfacial toughness and stability. The present investigation also show that an increase in porosity leads to significant modifications of the angular distribution of stress and velocity fields, together with a drastic reduction in the hydrostatic stress level, especially along the interfacial line. The asymptotic crack-tip fields obtained in the present paper could finally be used in conjunction with finite element simulations to perform a full-field analysis.

Acknowledgements

Financial support of MURST ex60% (2000) "Propagazione di fratture lungo l'interfaccia tra materiali duttili-porosi e fragili" is gratefully acknowledged.

References

Aoki, S., Kishimoto, K., Takeuchi, N., Sakata, M., 1992. An elastic–plastic finite element analysis of a blunting interface crack with microvoid damage. International Journal of Fracture 55, 363–374.

Bordia, R.K., Raj, R., 1985. Sintering behavior of ceramic films constrained by rigid substrate. Journal of the American Ceramic Society 68 (6), 287–292.

Bose, K., Mataga, P.A., Ponte Castañeda, P., 1999. Stable crack growth along a brittle/ductile interface – II. Small scale yielding solution and interfacial toughness predictions. International Journal of Solids and Structures 36 (1), 1–34.

Bose, K., Ponta Castañeda, P., 1992. Stable crack growth under mixed mode conditions. Journal of Mechanics Physics and Solids 40, 1053–1103.

Das, S., Wohlert, M., Beaman, J.J., Bourell, D.L., 1998. Producing metal part with selective laser sintering/hot isostatic pressing. JOM 50 (12), 17–20.

Drugan, W.J., 1991. Near-tip fields for quasi-static crack growth along a ductile–brittle interface. Journal of Applied Mechanics 58 (1), 111–119.

Drugan, W.J., Miao, Y., 1992. Influence of porosity on plane strain tensile crack-tip stress fields in elastic–plastic materials: part I. Journal of Applied Mechanics 59 (3), 559–567.

Drugan, W.J., Rice, J.R., 1984. Restrictions on quasi-statically moving surfaces of strong discontinuity in elastic–plastic solids. In: Dvorak, G.J., Shield, R.T. (Eds.), Mechanics of Material Behavior. Elsevier, Amsterdam, pp. 59–73.

Guo, Q., Keer, L.M., 1990. A crack at the interface between an elastic–perfectly plastic solid and a rigid substrate. Journal of Mechanics Physics and Solids 38 (6), 843–857.

Gurson, A.L., 1977. Continuum theory of ductile rupture by void nucleation and growth: part I – yield criteria and flow rules for porous ductile media. International Journal of Engineering Materials and Technology 99, 2–15.

Liechiti, K.M., Chai, Y.S., 1991. Biaxial loading experiments for determining interfacial toughness. Journal of Applied Mechanics 58, 680–687.

Liechiti, K.M., Chai, Y.S., 1992. Asymmetric shielding in interfacial fracture in-plane shear. Journal of Applied Mechanics 59, 295–304.

McCormack, T.M., Miller, R., Kesler, O., Gibson, L.J., 2001. Failure of sandwich beams with metallic foam cores. International Journal of Solids Structures 38, 4901–4920.

Miao, Y., Drugan, W.J., 1993. Influence of porosity on plane strain tensile crack-tip stress fields in elastic–plastic materials: part II. Journal of Applied Mechanics 60 (4), 883–889.

Miao, Y., Drugan, W.J., 1995. Asymptotic analysis of growing crack stress/deformation fields in porous ductile metals and implications for stable crack growth. International Journal of Fracture 72, 69–96.

Ponte Castañeda, P., Mataga, P.A., 1991. Stable crack growth along a brittle/ductile interface – I. Near-tip fields. International Journal of Solids Structures 27 (1), 105–133.

Radi, E., Bigoni, D., 1994. On crack propagation in porous hardening metals. International Journal of Plasticity 10 (7), 761–793.

Radi, E., Bigoni, D., 1996. Effects of anisotropic hardening on crack propagation in porous–ductile materials. Journal of Mechanics Phisics and Solids 44 (9), 1475–1508.

Tvergaard, V., 1990. Material failure by void growth to coalescence. Advances in Applied Mechanics 27, 83–151.

Williams, M.L., 1959. The stress around a fault or a crack in dissimilar media. Bulletin of Seismological Society of America 49 (2), 199–204.